Optical absorption and electron-nuclear double resonance study of Ni^{+} ions in $AgGaSe_2$ crystals

2004 J. Phys.: Condens. Matter 16 2593

(http://iopscience.iop.org/0953-8984/16/15/011)

INSTITUTE OF PHYSICS PUBLISHING JOURNAL OF PHYSICS: CONDENSED MATTER

J. Phys.: Condens. Matter **16** (2004) 2593–2607 PII: S0953-8984(04)73714-5

Optical absorption and electron-nuclear double resonance study of Ni^+ ions in $AgGaSe_2$ crystals

K T Stevens[1,4], N Y Garces[1], Lihua Bai[1], N C Giles[1], L E Halliburton[1,5], S D Setzler[2], P G Schunemann[2], T M Pollak[2], R K Route[3] and R S Feigelson[3]

[1] Department of Physics, West Virginia University, Morgantown, WV 26506, USA
[2] BAE Systems, Nashua, NH 03061, USA
[3] Center for Materials Research, Stanford University, Stanford, CA 94305, USA

E-mail: Larry.Halliburton@mail.wvu.edu

Received 19 December 2003
Published 2 April 2004
Online at stacks.iop.org/JPhysCM/16/2593
DOI: 10.1088/0953-8984/16/15/011

Abstract

Optical absorption, electron paramagnetic resonance (EPR) and electron-nuclear double resonance (ENDOR) have been used to characterize Ni^+ ions substituting for Ag^+ ions in $AgGaSe_2$ crystals. These Ni^+ ions are responsible for a strongly polarized optical absorption band peaking near 2.2 μm (the maximum absorption occurs with $E \parallel c$). Phonon structure is resolved at low temperature. This infrared band, which is present even in undoped crystals because of trace amounts of Ni, can significantly degrade the performance of optical parametric oscillators using $AgGaSe_2$. Sets of EPR and ENDOR angular dependence data were taken in the (010), ($\bar{1}$10) and (001) planes. This allowed the g matrix, the ^{61}Ni hyperfine and nuclear quadrupole matrices, the ^{77}Se hyperfine matrix for the four nearest neighbours and the ^{69,71}Ga hyperfine and nuclear quadrupole matrices for four neighbours to be determined. Of the eight gallium near neighbours, only the four in the basal plane containing the Ni^+ ion have a significant interaction. Large hyperfine interactions with ^{107,109}Ag nuclei were not observed.

1. Introduction

Silver gallium selenide ($AgGaSe_2$) is a well-known I–III–VI_2 compound semiconductor that crystallizes in the chalcopyrite structure. The Ag and Ga ions each have four Se ions as nearest neighbours, and the Se ions have two Ag and two Ga ions as nearest neighbours. In general,

[4] Present address: Northrop Grumman Space Technology, Synoptics, Charlotte, NC 28273, USA.
[5] Author to whom any correspondence should be addressed.

the I–III–VI_2 chalcopyrites are analogous to the II–VI zinc blende compounds. Because of its sufficient birefringence, high transmission and large nonlinear optical coefficient, $AgGaSe_2$ is an attractive material for second harmonic generation (SHG) and optical parametric oscillator (OPO) applications in the mid-infrared [1–3]. However, the introduction of point defects (e.g., impurities, vacancies, antisites, etc) during crystal growth or subsequent fabrication can have a significant effect on the operation of these nonlinear optical devices. Absorption bands associated with the point defects may overlap either the pump or the output beams, and thus degrade the performance of the optical device.

An extrinsic e-polarized absorption band near 2.2 μm is present in most single crystals of $AgGaSe_2$ [4]. This band overlaps the desired 2 μm pump wavelength, and directly affects the performance of $AgGaSe_2$-based OPOs. Catella *et al* [4] investigated a set of 23 crystals grown over a six-year period and found that the 2.2 μm absorption band varied from sample to sample by over an order of magnitude, thus indicating the absorption is due to an extrinsic defect. These investigators were unable to make a precise identification of the responsible defect, but they did suggest that it was perhaps associated with deviations from stoichiometry. In a subsequent study, Halliburton *et al* [5] made a direct analogy to earlier work by Kaufmann [6] on $AgGaS_2$ and assigned the 2.2 μm absorption band in $AgGaSe_2$ to Ni^+ ($3d^9$) impurities that were unintentionally present in the crystals. More recently, a theoretical investigation of the g factors and hyperfine parameters of Ni^+ ions in $AgGaS_2$ and $AgGaSe_2$ has been reported [7].

In the present paper, we describe the results of an optical absorption, electron paramagnetic resonance (EPR) and electron-nuclear double resonance (ENDOR) study of Ni^+ ions substituting for Ag^+ ions in $AgGaSe_2$ crystals. Intentional doping with Ni during growth causes the highly polarized infrared absorption band near 2.2 μm to increase significantly. At 10 K, this band exhibits an easily resolved phonon structure arising from a local vibrational mode. The ENDOR spectra from these isolated Ni^+ ions provide spin Hamiltonian parameters for the ^{61}Ni nucleus, the four neighbouring ^{77}Se nuclei and four of the eight neighbouring ^{69,71}Ga nuclei. Following the approach of Kaufmann [6], we relate the EPR g matrix to the optical absorption spectra and determine the relative positions of the crystal-field split energy levels of the Ni^+ ($3d^9$) ion in the tetragonal symmetry of the $AgGaSe_2$ crystal.

2. Crystal structure

The tetragonal symmetry of the $AgGaSe_2$ crystal is described by the space group $I\bar{4}2d$. There are eight atoms in the unit cell. As customary, the unique axis is labelled the c axis (or [001] direction) and the two equivalent axes in the basal plane are labelled the a axes (or [100] and [010] directions). Room temperature values for the lattice parameters are $a = 5.991$ Å and $c = 10.885$ Å [8]. The resulting c/a ratio is 1.82, which indicates that there is significant compression of the lattice along the c axis. Atom positions in the I–III–VI_2 chalcopyrite structure can be generated using the following minimum set of (x, y, z) coordinates (expressed in units of the a and c lattice constants):

Group I: (0,0,0), $(0, \frac{1}{2}, \frac{1}{4})$
Group III: $(0, 0, \frac{1}{2})$, $(0, \frac{1}{2}, \frac{3}{4})$
Group VI: $(x, \frac{1}{4}, \frac{1}{8})$, $(-x, \frac{3}{4}, \frac{1}{8})$, $(\frac{3}{4}, x, \frac{7}{8})$, $(\frac{1}{4}, -x, \frac{7}{8})$.

The parameter x has a room-temperature value of 0.2828 for $AgGaSe_2$ [9]. It is a measure (when compared to 1/4) of the relative rotations of the anion 'tetrahedra' about the cation sites [10]. This small shifting in position of the selenium ions occurs because the silver and gallium ions have different 'effective' radii and, thus, different bond lengths with the neighbouring seleniums (i.e. the Ag–Se separation is greater than the Ga–Se separation). A

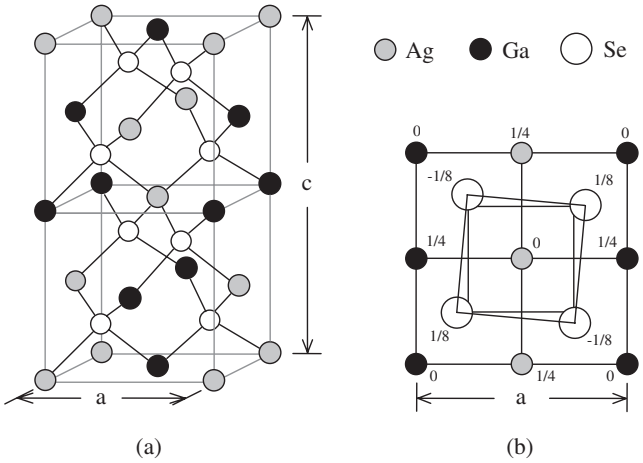

Figure 1. (a) A general view of the chalcopyrite crystal structure. (b) Projection of the $AgGaSe_2$ lattice on the *c* plane, illustrating the relative shifts of the four selenium neighbours around one of the two crystallographically equivalent silver sites. The numbers next to the ions are their *z* coordinates (in units of the *c* lattice constant).

general view of the chalcopyrite crystal structure is provided in figure 1(a), and a more detailed view of the selenium shifts about a silver ion in $AgGaSe_2$ is shown in figure 1(b). In EPR and ENDOR studies, it is often instructive to compare the principal-axis directions of the hyperfine matrices with actual ion-to-ion directions in the lattice. Thus we used the above expressions, along with lattice translations, to obtain the positions of a subset of ions that are relevant to our study of Ni^+ substituting for Ag^+. Table 1 lists the coordinates for the four Se and eight Ga nearest-neighbour ions that surround each of the two crystallographically equivalent Ag positions.

3. Experimental details

The $AgGaSe_2$ crystals used in the present investigation were grown by the horizontal Bridgman technique at BAE Systems (Nashua, NH) and by the vertical Bridgman technique at Stanford University (Palo Alto, CA). In the heaviest doped boule, elemental nickel at a level of 1600 ppm was added to the starting material and the final concentration in this crystal was estimated from the intensity of the EPR signal to be greater than 1000 ppm. Other boules were grown with reduced doping levels or with no intentional doping. In all cases, the boules were subjected to post-growth anneals in the presence of Ag_2Se to minimize internal scattering centres [11–13]. Small samples for our spectroscopic studies were cut from the larger boules. The samples for optical absorption were *a*-axis plates with approximate dimensions of $2.6 \times 6 \times 6$ mm^3, and were mechanically polished on the broad faces. The EPR/ENDOR samples were nearly cubic in shape with approximate dimensions of $2 \times 3 \times 3$ mm^3 (the faces were perpendicular to the *a* and *c* high-symmetry directions).

The infrared optical absorption data were taken with a Nicolet Magna 550 FTIR spectrometer while using an Optistat helium flow system from Oxford Instruments to control the sample temperature. When measuring the polarization dependence, a ZnSe wire-grid polarizer from Molectron (Model IGP-229) was placed in the incident beam path of the spectrometer. The EPR and ENDOR data were obtained using a Bruker Instruments ESP-300 spectrometer operating near 9.5 GHz. A Bruker cylindrical TE_{011} ENDOR cavity (with internal coil) was used for all measurements. An Oxford Instruments ESR-900 helium-gas-

Table 1. Positions of Se and Ga atoms surrounding the two crystallographically equivalent Ag sites in $AgGaSe_2$. The first set of 13 atoms have Ag(1) at the centre and the second set of 13 have Ag(2) at the centre. Five atoms are common to the two sets. Specifically, the Se(1), Ga(1), Ga(2), Ga(5) and Ga(6) positions also appear in the second set.

Atom	x (Å)	y (Å)	z (Å)
Set number 1, atoms surrounding Ag(1)			
Ag(1)	0.0	0.0	0.0
Se(1)	1.694	1.498	1.361
Se(2)	−1.694	−1.498	1.361
Se(3)	−1.498	1.694	−1.361
Se(4)	1.498	−1.694	−1.361
Ga(1)	2.995	2.995	0.0
Ga(2)	−2.995	2.995	0.0
Ga(3)	−2.995	−2.995	0.0
Ga(4)	2.995	−2.995	0.0
Ga(5)	2.995	0.0	2.721
Ga(6)	−2.995	0.0	2.721
Ga(7)	0.0	−2.995	−2.721
Ga(8)	0.0	2.995	−2.721
Set number 2, atoms surrounding Ag(2)			
Ag(2)	0.0	2.995	2.721
Se(5)	1.694	1.498	1.361
Se(6)	−1.694	4.493	1.361
Se(7)	−1.498	1.301	4.082
Se(8)	1.498	4.690	4.082
Ga(9)	2.995	0.0	2.721
Ga(10)	−2.995	0.0	2.721
Ga(11)	2.995	5.991	2.721
Ga(12)	−2.995	5.991	2.721
Ga(13)	0.0	0.0	5.442
Ga(14)	0.0	5.991	5.442
Ga(15)	2.995	2.995	0.0
Ga(16)	−2.995	2.995	0.0

flow system maintained the sample temperature at selected values in the 10–20 K range. The magnetic field was amplitude modulated at 25 kHz during the EPR measurements, and the rf field was frequency modulated at 12.5 kHz during the ENDOR measurements. Values of the static magnetic field were obtained with a proton gaussmeter. A small Cr-doped MgO crystal was used to correct for the difference in magnetic field between the sample and the probe tip of the gaussmeter (the isotropic g value for Cr^{3+} in MgO is taken to be 1.9800).

4. Results

Both undoped and Ni-doped $AgGaSe_2$ crystals were included in our study. In the undoped crystals, Ni impurities were present at trace levels of a few ppm and we could easily observe EPR signals from both Ni^+ and Ni^{3+} ions. Changes in the relative concentrations of these two charge states could be photoinduced at low temperature. In contrast, the Ni^+ ions were dominant in the Ni-doped crystals and we did not observe an EPR signal from Ni^{3+} ions. Because of the larger concentration of Ni^+ in the doped crystals and the resulting larger ENDOR signals, we only report data taken on the heaviest doped crystals.

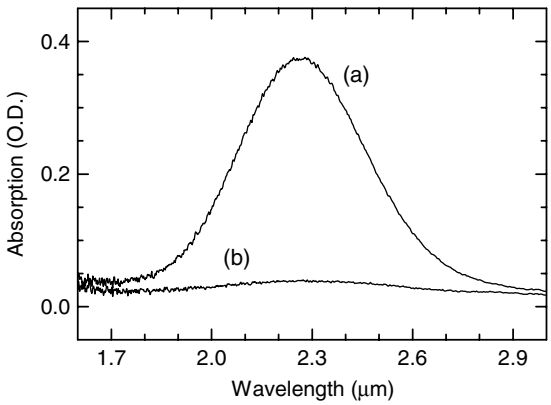

Figure 2. Polarized optical absorption from Ni^+ ions in $AgGaSe_2$. (a) $E \parallel c$ and (b) $E \perp c$. These data were taken at room temperature with light propagating along the [100] direction. The sample thickness was 2.6 mm.

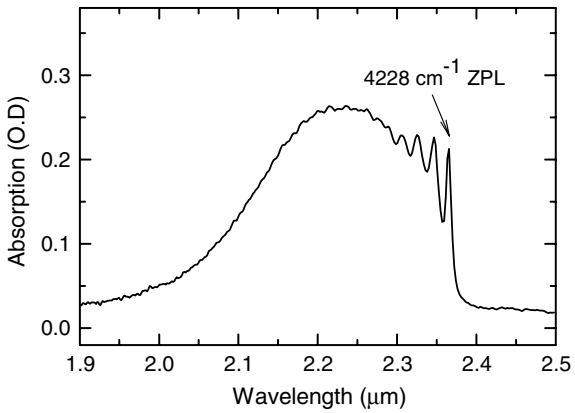

Figure 3. Optical absorption of Ni^+ ions taken at 10 K with unpolarized light propagating along the [100] direction. The phonon structure is observed at this temperature.

4.1. Optical absorption and EPR

An optical absorption spectrum of Ni^+ in $AgGaSe_2$, taken at room temperature, is shown in figure 2 for e-polarized ($E \parallel c$) and o-polarized ($E \perp c$) light. This absorption is strongly polarized with a maximum occurring when the incident light has its electric field vector parallel to the c axis of the crystal. The peak of the band occurs at 2.25 μm. The phonon structure emerges on this band when the temperature is lowered, as illustrated in figure 3. These data in figure 3 were taken at 10 K with unpolarized light. The zero-phonon line is at 4228 cm^{-1} (2.365 μm) and the one-phonon line is at 4262 cm^{-1}, giving a 34 cm^{-1} separation. The two- and three-phonon lines are also seen in figure 3 with this same separation. Using this local phonon energy (which does not coincide with any reported lattice phonons in $AgGaSe_2$), we found that the peak in the absorption near 4444 cm^{-1} (i.e. 2.25 μm) corresponds to a Huang–Rhys factor of about 7. We also observed a second and much less intense set of lines in our Ni-doped samples. At 10 K, a zero-phonon line is located at 3726 cm^{-1}, with associated one-phonon and two-phonon lines at 3760 and 3794 cm^{-1}. These weak lines have their maximum intensity when the electric field vector is perpendicular to the c axis of the

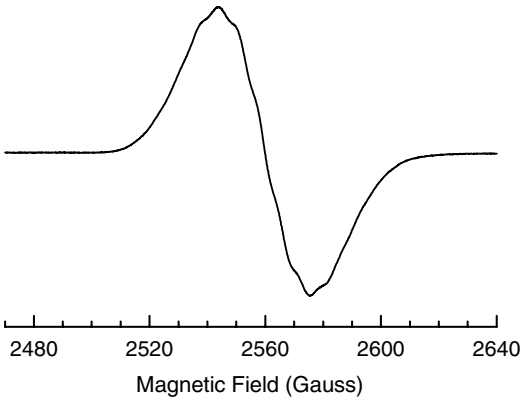

Figure 4. EPR spectrum of Ni^+ ions in $AgGaSe_2$. These data were taken at 10 K with the magnetic field parallel to the [001] direction. The microwave frequency was 9.476 GHz.

crystal. The 34 cm^{-1} separation, representing the local phonon energy, matches that found for the more intense set of lines shown in figure 3. Since the two sets of absorption lines exhibit identical local couplings to the lattice, they are very likely due to the same centre, i.e. a Ni^+ ion. The origin of these two Ni^+ transitions is described in the discussion section. Kaufmann [6] has observed similar structure at low temperature for Ni^+ in $AgGaS_2$, including zero-phonon lines at 4686 and 3526 cm^{-1} and a local-phonon frequency near 42 cm^{-1}. It is interesting to note that the ratio of the experimental local-phonon frequencies associated with Ni^+ ions in $AgGaS_2$ and $AgGaSe_2$ is 1.24, and a simple harmonic oscillator model based on the reduced masses of Ni–S and Ni–Se vibrating systems predicts 1.27. This agreement confirms that these local modes are vibrations involving the Ni^+ ion and its nearest neighbour anions.

A relatively broad (32 G) and very intense single EPR line was present in the as-grown Ni-doped $AgGaSe_2$ crystals. This signal is shown in figure 4. These data were taken at 10 K with the magnetic field parallel to the *c* axis of the crystal. Halliburton *et al* [5] have previously assigned this EPR spectrum to Ni^+ ions substituting for Ag^+ ions in the $AgGaSe_2$ lattice. The slightly resolved hyperfine pattern in figure 4, observable only with the magnetic field parallel to the *c* axis, was tentatively assigned in that earlier work to four equivalent gallium neighbours. In our present investigation, the angular dependence of this EPR signal was recorded in three planes (the magnetic field was rotated from the [001] direction to the [100] direction in the (010) plane, from the [001] direction to the [110] direction in the $(\bar{1}10)$ plane, and from the [100] direction to the [110] direction in the (001) plane). During these rotations, the EPR signal from the Ni^+ ions always remained in one line, i.e. there was no observed splitting due to magnetically inequivalent sites. Furthermore, the line did not shift in position when the magnetic field was rotated in the (001) plane. These results for the $(\bar{1}10)$ and (001) planes are shown in figure 5. In order to acquire accurate in-plane EPR data, the EPR and ENDOR measurements were made simultaneously because both the ^{77}Se and $^{69,71}Ga$ ENDOR lines (as described later) showed site splittings and could be used for alignment. The following spin Hamiltonian was used to fit the EPR angular data.

$$\mathbf{H} = \beta \mathbf{S} \cdot \mathbf{g} \cdot \mathbf{B}. \tag{1}$$

A total of 40 data points (pairs of magnetic field and microwave frequency) from the three rotation planes were included. The unique axis of the *g* matrix is oriented along the [001] direction of the crystal, and the 'best fit' values for $g_\parallel$ and $g_\perp$ are given in table 2. These results are in agreement with the earlier work of Halliburton *et al* [5].

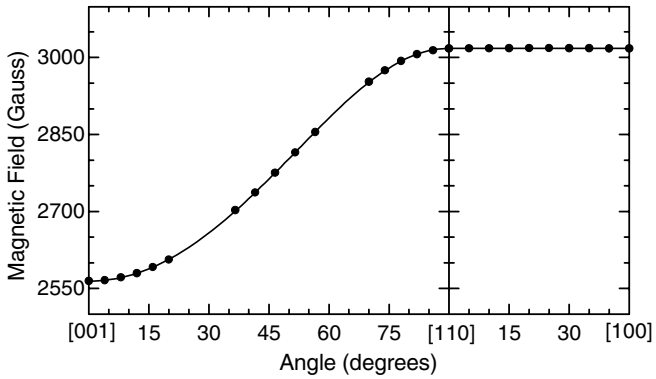

Figure 5. Angular dependence of the Ni^+ EPR spectrum. Results are presented for the $(\bar{1}10)$ plane and the (001) plane. The discrete points represent experimental data and the smooth curves are computer-generated using best-fit parameters.

Table 2. Principal values and principal axis directions of the g matrix, the hyperfine matrices and the nuclear quadrupole matrices associated with isolated Ni^+ centres in $AgGaSe_2$. The principal-axis directions for the ^{77}Se and ^{69}Ga nuclei correspond to one of the symmetry-related neighbouring sites. Error limits are ± 0.0005 for the g values, ± 0.1 MHz for the ^{61}Ni and ^{77}Se A values and the ^{61}Ni Q value, ± 0.03 MHz for the ^{69}Ga A values, ± 0.002 MHz for the ^{69}Ga Q values, and $\pm 1^\circ$ for the θ and ϕ angles.

			Principal axes	
	Principal values		θ (deg)	ϕ (deg)
g	$g_\parallel$	2.6470	0	0
	$g_\perp$	2.2493		
A (^{61}Ni)	$A_\parallel$	-60.2 MHz	0	0
	$A_\perp$	-88.2 MHz		
Q (^{61}Ni)	Q_{zz}	-11.0 MHz	0	0
	$(Q_{xx} = Q_{yy} = -\frac{1}{2}Q_{zz})$			
A (^{77}Se)	A_1	+36.1 MHz	118	351
	A_2	+38.6 MHz	78	267
	A_3	+68.6 MHz	149	197
A (^{69}Ga)	A_1	+19.89 MHz	59	156
	A_2	+20.63 MHz	93	244
	A_3	+22.27 MHz	31	329
Q (^{69}Ga)	Q_1	+0.471 MHz	80	47
	Q_2	+0.031 MHz	66	142
	Q_3	-0.502 MHz	26	296

4.2. Nickel (^{61}Ni) ENDOR

The ^{61}Ni nucleus ($I = 3/2$, 1.13% abundant) is responsible for the largest hyperfine interaction in the ENDOR spectra from Ni^+ in $AgGaSe_2$. We were able to detect the ENDOR signals from these ^{61}Ni nuclei in our Ni-doped samples, despite the low natural abundance, and thus there was no need to grow crystals enriched with the ^{61}Ni isotope. Figure 6 shows the ^{61}Ni ENDOR spectrum taken at 10 K with the magnetic field along the [110] direction. This spectrum consists of two sets of three lines (as indicated by the 'stick' diagram in figure 6) with the three lines in each set caused by a large nuclear quadrupole interaction. The angular dependence of

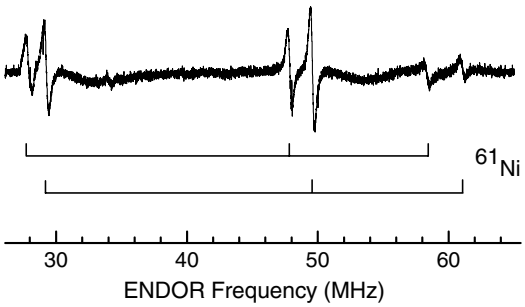

Figure 6. ENDOR spectrum of ^{61}Ni taken at 10 K with the magnetic field (3015.7 G) aligned along the [110] direction. There are two sets of three lines each, as illustrated by the lower stick diagrams.

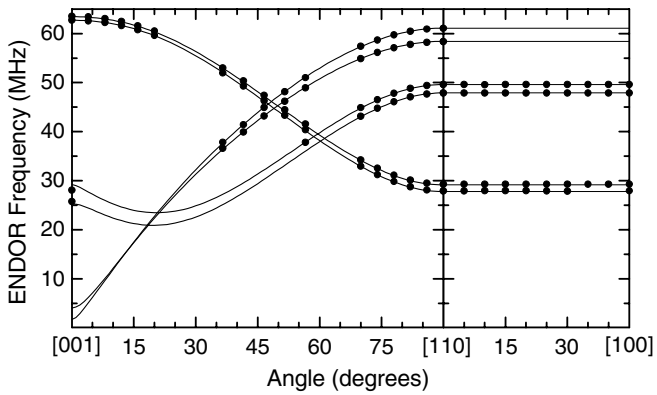

Figure 7. Angular dependence of the ^{61}Ni ENDOR spectrum. Results are presented for the $(\bar{1}10)$ plane and the (001) plane. The discrete points represent experimental data and the smooth curves are computer-generated using the best-fit parameters.

the ^{61}Ni ENDOR lines was recorded in the $(\bar{1}10)$ plane and in the (001) plane. These results are represented in figure 7 by the discrete data points. In the regions where experimental data points are not shown, either the signals were less than or comparable to the noise, or there was interference from ^{77}Se and ^{69,71}Ga signals.

The following spin Hamiltonian was used to fit the ^{61}Ni ENDOR angular data.

$$\mathbf{H} = \beta \mathbf{S} \cdot \mathbf{g} \cdot \mathbf{B} + \mathbf{I} \cdot \mathbf{A} \cdot \mathbf{S} + \mathbf{I} \cdot \mathbf{Q} \cdot \mathbf{I} - g_N \beta_N \mathbf{I} \cdot \mathbf{B}. \tag{2}$$

These terms represent the electron Zeeman, hyperfine, nuclear quadrupole and nuclear Zeeman interactions, respectively. The angular dependence in figure 7 suggests that the hyperfine and nuclear quadrupole matrices are axial with the unique axis parallel to the [001] direction (in agreement with the earlier result for the g matrix). This, then, requires only two hyperfine parameters ($A_\parallel$ and $A_\perp$) and one nuclear quadrupole parameter (Q_{zz}). The $\mathbf{Q}$ matrix is traceless and the other two principal values in the case of ^{61}Ni are $Q_{xx} = -Q_{zz}/2$ and $Q_{yy} = -Q_{zz}/2$. Values for the three ^{61}Ni parameters were obtained by fitting 86 data points (each representing a magnetic field and an rf frequency) from the two rotation planes. These results are included in table 2. We do not have direct information about the absolute signs for the spin-Hamiltonian parameters (only relative signs are known from experiment). Theoretical predictions for Ni^+ in $AgGaS_2$ [7], however, have suggested that $A_\parallel$ and $A_\perp$ have negative signs, and this also agrees with the negative sign of the ^{61}Ni nuclear magnetic moment. For these reasons, we

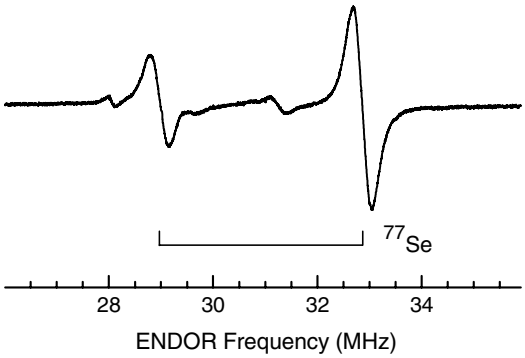

Figure 8. ENDOR spectrum of ^{77}Se taken at 9 K with the magnetic field (2563.3 G) along the [001] direction. All four selenium neighbours are equivalent for this orientation of field. The small line at 28.1 MHz is a direct transition of the ^{61}Ni nucleus, while the small line at 31.3 MHz is a harmonic of the ^{61}Ni transition at 62.6 MHz.

tentatively assign negative signs to $A_\parallel$ and $A_\perp$ in table 2. We note that the principal values of an axial quadrupole matrix are often expressed in terms of a parameter P (i.e. $Q_{xx} = -P$, $Q_{yy} = -P$ and $Q_{zz} = 2P$). This parameter P is defined as $e^2qQ/[4I(2I-1)]$, where eq is the electric field gradient and Q is the nuclear quadrupole moment.

4.3. Selenium (^{77}Se) ENDOR

The Ni^+ ions in $AgGaSe_2$ occupy a Ag^+ lattice site and are bonded to four selenium ions. Hyperfine interactions with the subset of ^{77}Se nuclei ($I = 1/2$, 7.6% abundant) among these neighbours give rise to ENDOR lines in the 16–36 MHz region. Since there are four selenium neighbours, the probability of a Ni^+ ion having one neighbouring ^{77}Se nucleus is 24.0%. The Ni^+ ion is smaller than the Ag^+ ion, and we initially thought that this would allow the Ni^+ ion to move to a slightly off-centre position and thus cause inequivalent interactions with these seleniums. However, our ENDOR data show that all four selenium neighbours are equivalent, and we conclude that no additional distortion occurs when the Ni^+ ion replaces the Ag^+ ion, other than a possible symmetrical inward relaxation of the four seleniums.

As expected, the ENDOR spectra from these nearest neighbours do show site splittings. Because there are two magnetically inequivalent, but crystallographically equivalent, sites for each cation in the chalcopyrite structure, and since each cation is bonded to four anions (selenium in our case), there will be eight magnetically inequivalent, but crystallographically equivalent, anion sites. In our ENDOR spectra, all eight selenium sites are equivalent when the magnetic field is along the [001] direction. These eight sites separate into two sets of four equivalent sites each when the magnetic field is along the [100] direction and the [110] direction (note that the combinations of sites comprising these sets are different for the two directions). There are four sets of distinguishable sites (each doubly degenerate) when the magnetic field is rotated in the (010), ($\bar{1}$10) and (001) planes. Rotation out of these planes is easily detected when this double degeneracy of lines is removed in the ^{77}Se ENDOR spectra.

Figure 8 shows the ^{77}Se ENDOR spectrum taken at 9 K with the magnetic field along the [001] direction in the crystal. The magnitude of the magnetic field was 2563.3 G and the two lines are centred on 30.91 MHz and split by 3.89 MHz. This observed splitting agrees with the expected $2\nu_N$ value of 4.179 MHz for this field, thus verifying that ^{77}Se is the responsible nucleus. The angular dependence of the ^{77}Se ENDOR lines was recorded in the (010), ($\bar{1}$10)

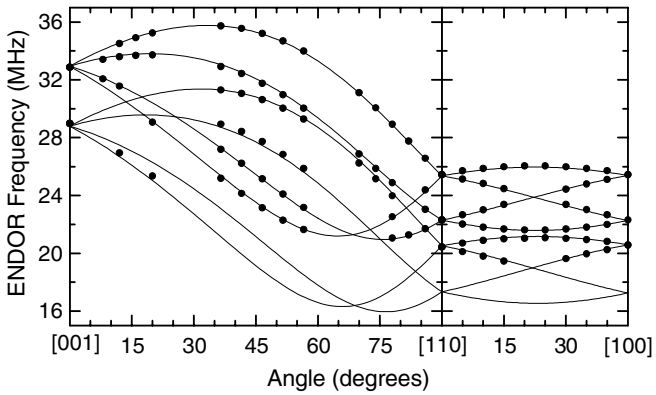

Figure 9. Angular dependence of the ^{77}Se ENDOR spectra. Results are presented for the $(\bar{1}10)$ plane and the (001) plane. The discrete points represent experimental data and the smooth curves are computer-generated using the best-fit parameters.

and (001) planes. Figure 9 shows this angular dependence for the $(\bar{1}10)$ plane and the (001) plane. A lack of data points in the lower portion of figure 9 (the 16–18 MHz region) is caused by interference from ^{71}Ga ENDOR lines.

The spin Hamiltonian in equation (2), without the nuclear quadrupole term, was used to fit the ^{77}Se ENDOR angular data. Six parameters (three principal values and three Euler angles to describe the directions of the principal axes) are required to completely specify the hyperfine matrix. The values of the ^{77}Se parameters were determined by fitting a total of 202 ENDOR line positions (i.e. frequencies and their associated magnetic field values) from the three rotation planes. These results are presented in table 2. The principal values are given positive signs in table 2 because the ^{77}Se nuclear magnetic moment has a positive sign (we have not experimentally verified this assignment). Instead of using the three Euler angles to specify the directions of the principal axes for the ^{77}Se hyperfine matrix, we use pairs of angles (θ, ϕ) where the polar angle θ is measured relative to the c axis and the azimuthal angle ϕ is measured relative to the a axis in the c plane with positive rotation from a to b.

The principal-axis directions given in table 2 correspond to only one of the eight possible sites for the ^{77}Se nuclei. The principal values are the same for each of the eight sites, but the principal-axis directions vary for each site since they must reflect the symmetry elements of the $AgGaSe_2$ lattice. The pairs of angles needed to describe the directions of each of the principal axes at the other seven sites can be obtained from the initial site by using the following reflections and rotations. In some of these transformations, a right-hand coordinate system is not retained.

Site 1:	(θ, ϕ)	
Site 2:	$(\theta, 180° + \phi)$	Site 1 rotated by 180° about c
Site 3:	$(180° - \theta, 90° + \phi)$	Site 1 reflected through basal plane and rotated 90° about c
Site 4:	$(180° - \theta, 270° + \phi)$	Site 3 rotated by 180° about c
Site 5:	$(180° - \theta, 360° - \phi)$	Site 1 rotated by 180° about a
Site 6:	$(180° - \theta, 180° - \phi)$	Site 2 rotated by 180° about a
Site 7:	$(\theta, 90° - \phi)$	Site 3 rotated by 180° about b
Site 8:	$(\theta, 270° - \phi)$	Site 4 rotated by 180° about b

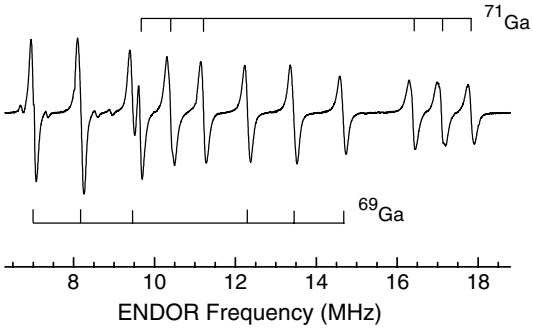

Figure 10. ENDOR spectrum of the basal plane ^{69}Ga and ^{71}Ga nuclei taken at 9 K with the magnetic field (2563.3 G) aligned along the [001] direction. All four of the gallium sites are equivalent for this orientation of magnetic field.

4.4. Gallium (^{69}Ga) ENDOR

A Ni^+ ion substituting for a Ag^+ ion in $AgGaSe_2$ has eight neighbouring gallium ions. These divide into two sets of four ions each, with one set of gallium ions located in the basal plane (each of these gallium ions is 4.236 Å from the Ni^+ ion if no lattice distortion is present) and the other set located in pairs above and below the basal plane (each of these gallium ions is 4.046 Å from the Ni^+ ion in the absence of lattice distortion). The two sets of gallium neighbours are clearly inequivalent for all angles of magnetic field. Large ENDOR signals due to hyperfine and quadrupole interactions with ^{69}Ga ($I = 3/2$, 60.1% abundant) and ^{71}Ga ($I = 3/2$, 39.9% abundant) nuclei are observed between 6 and 19 MHz. These signals come from only one set of four gallium neighbours (i.e. one of the two inequivalent neighbouring sets). The other set of four gallium neighbours must have smaller hyperfine interactions, and they probably contribute to the large number of ENDOR lines observed below 6 MHz that were not analysed in the present study. We assign the gallium ENDOR lines in the 6–19 MHz region to the set of four gallium sites located in the basal plane of the Ni^+ ion, since the unpaired spin in this $3d^9$ system is expected to have lobes extending out toward these ions (i.e. the spin is primarily in an $|xy\rangle$-like orbital).

Figure 10 shows the ^{69}Ga and ^{71}Ga ENDOR spectra taken at 9 K with a magnetic field of 2563.3 G along the [001] direction in the crystal. Each isotope is represented by a pair of triplets (because of the nuclear quadrupole interaction). The angular dependences of the ^{69}Ga and ^{71}Ga ENDOR lines were recorded in the (010), ($\bar{1}$10) and (001) planes. In figure 11, we show the angular dependence of the ^{69}Ga spectrum in the ($\bar{1}$10) plane and the (001) plane. The spin Hamiltonian in equation (2) was used to fit the complete set of ^{69}Ga data (all three planes). Eleven parameters (six for the hyperfine matrix and five for the nuclear quadrupole matrix) are needed to describe the angular dependence data for one isotope. The values of the ^{69}Ga parameters were determined by fitting a total of 432 ENDOR lines (i.e. frequencies and associated magnetic field values) taken from the three rotation planes. These results are listed in table 2. The principal values are given positive signs in table 2 (without experimental verification) because the ^{69}Ga nuclear magnetic moment has a positive sign. We again use pairs of angles (θ, ϕ) to specify the directions of the principal axes. Analogous results were obtained for the ^{71}Ga nuclei, but are not listed in table 2.

5. Discussion

The unpaired spin in our $3d^9$ system resides primarily in the $|xy\rangle$-like orbital, with lobes in the (001) basal plane (extending out in the [110] directions). Our ENDOR results show that there

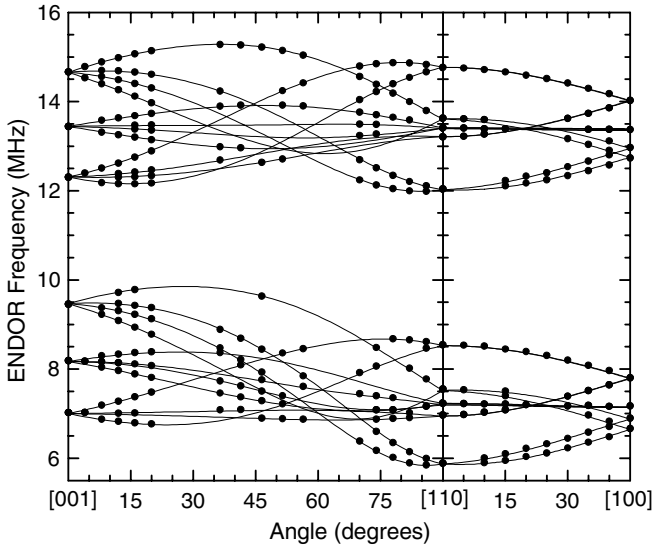

Figure 11. Angular dependence of the ^{69}Ga ENDOR spectra. Results are presented for the $(\bar{1}10)$ plane and the (001) plane. The discrete points represent experimental data and the smooth curves are computer-generated using the best-fit parameters.

is considerable overlap of the Ni^+ wavefunction onto the neighbouring ions. The principal values of the selenium and gallium hyperfine matrices (given in table 2) can be separated into isotropic and anisotropic components using $\mathbf{A} = a\mathbf{I}+\mathbf{B}$ where a is the Fermi contact term and $\mathbf{B}$ is the dipole–dipole interaction with b and b' representing the axial and nonaxial contributions, respectively.

$$\mathbf{B} = \begin{pmatrix} -b-b' & 0 & 0 \\ 0 & -b+b' & 0 \\ 0 & 0 & 2b \end{pmatrix}. \tag{3}$$

For the ^{77}Se neighbours, this gives $a = +47.77$ MHz, $b = +10.42$ MHz and $b' = -1.25$ MHz. From these values, we can make an approximate estimate of the amount of unpaired spin on these nearest neighbour selenium ions. Using free-atom values of $a = 20\,102$ MHz and $b = 491.2$ MHz for the valence 4s and 4p orbitals of selenium [14, 15], we estimate that 9.5% of the Ni^+ unpaired spin is on the four neighbouring seleniums (8.5% in the 4p orbitals and 1.0% in the 4s orbitals). A similar analysis using the ^{69}Ga principal hyperfine values in table 2 suggests that, at a minimum, 2.0% of the unpaired spin is on the four basal-plane gallium ions (1.3% in the 4p orbitals and 0.7% in the 4s orbitals). Combining these results and allowing for smaller overlaps onto additional neighbours, we conclude that approximately 88% of the unpaired spin is localized on the central nickel ion.

The direction of the unique principal axis of the selenium hyperfine matrix (i.e. the axis associated with the 68.6 MHz principal value) provides evidence that the unpaired spin resides primarily in the $|xy\rangle$ orbital of the Ni^+ ion. We suggest that the set of ^{77}Se principal axes given in table 2 corresponds to the ion labelled Se(1) in table 1. The unique principal axis at this site points down from the selenium ion toward the adjacent lobe of the $|xy\rangle$ orbital extending out in the [110] direction. Specifically, the intersection of this principal axis with the basal plane occurs at $x = 0.91$ Å and $y = 1.26$ Å, if the lattice relaxation of the selenium ions surrounding the Ni^+ ion is not taken into account. Because of its close proximity to the

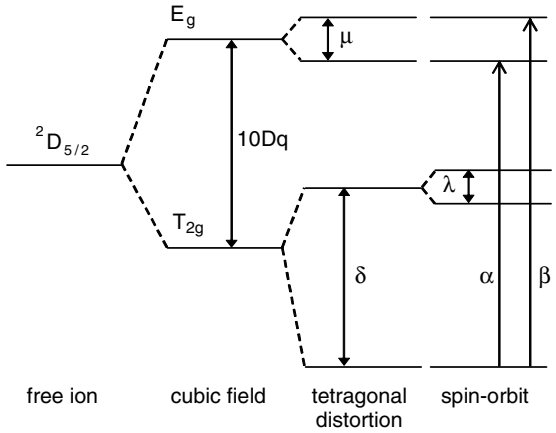

Figure 12. Energy level diagram for Ni^+ ($3d^9$) ions in $AgGaSe_2$. The figure is drawn approximately to scale using the calculated values of the $10Dq$, δ, μ and λ parameters.

selenium ion, this nearest $|xy\rangle$ lobe is the governing factor in determining the direction of the selenium unique principal axis. The rotation of the anion tetrahedron about the c axis in the chalcopyrite structure (discussed in section 2) makes the ϕ angle for this principal-axis direction have a value slightly less than 225° (it has an experimental value of 197° in table 2). In the case of the ^{69}Ga hyperfine and quadrupole matrices, the situation is more complex and we were unable to assign the sets of principal axes in table 2 to a particular gallium site (i.e. ion in table 1).

Kaufmann [6], in his study of Ni^+ in $AgGaS_2$, provided a complete analysis of the g factors and hyperfine constants associated with the ground state of a substitutional d^9 ion. This was done for the case when the tetragonal distortion and the spin–orbit coupling are of the same order. A similar analysis of the g factors for a d^1 spin system has been described by Wertz and Bolton [16]. As shown in figure 12, the $^2D_{5/2}$ ground state of a Ni^+ ion is split into five Kramers doublets by the static crystal field and the spin–orbit coupling. This energy level scheme is characterized by the four parameters $10Dq$, μ, δ and λ. Two distinct zero-phonon infrared transitions, labelled α and β in figure 12, are observed at 3726 and 4228 cm^{-1}, respectively, in our optical absorption spectra of Ni^+ in $AgGaSe_2$. The β band is much more intense than the α band, and they have opposite polarizations. A small transition probability along with interference from other unrelated weak absorption bands made it difficult to identify the α band in the absorption spectra, but our observation of the 34 cm^{-1} phonon structure on the α band leaves no doubt about our assignment.

Expressions for the g values and the ^{61}Ni hyperfine parameters are given below [6].

$$g_\parallel = g_e \cos 2\omega - 2k \sin^2\omega - \left(\frac{4k\lambda_0}{\Delta}\right)\left(2\cos^2\omega + \frac{1}{2}\sqrt{2}\sin 2\omega\right) \tag{4}$$

$$g_\perp = g_e \cos^2\omega - \sqrt{2}k \sin 2\omega + \left(\frac{\sqrt{2}k\lambda_0}{\Delta}\right)\left(\sin 2\omega + \sqrt{2}\sin^2\omega\right) \tag{5}$$

$$A_\parallel = P\left[-\tfrac{4}{7} + 2\left(\tfrac{1}{7} - k\right)\sin^2\omega - \kappa\cos 2\omega - \tfrac{3}{7}\sqrt{2}\sin 2\omega - \left(\frac{4\lambda'}{\Delta}\right)\left(2k'\cos^2\omega + \frac{3}{14}\sin^2\omega + \frac{1}{28}\sqrt{2}\left(3 + 14k'\right)\sin 2\omega\right)\right] \tag{6}$$

$$A_\perp = P\Big[\big(\tfrac{2}{7}-\kappa\big)\cos^2\omega - \sqrt{2}\big(k-\tfrac{3}{14}\big)\sin 2\omega - \left(\frac{\sqrt{2}\lambda'}{\Delta}\right)\left(\frac{3}{14}-k'\right)\big(\sin 2\omega + \sqrt{2}\sin^2\omega\big)\Big]. \tag{7}$$

The free-ion spin–orbit coupling constant for Ni^+ is $\lambda_0 = -605\ cm^{-1}$, and the orbital reduction factors are k and k' (i.e. $\lambda = k\lambda_0$, $\lambda' = k'\lambda_0$ and $k' = \sqrt{k}$). The parameter ω is defined by

$$\sin 2\omega = \sqrt{2}\eta/S \tag{8}$$

where

$$S = \big[\big(1+\tfrac{1}{2}\eta\big)^2 + 2\eta^2\big]^{1/2} \qquad \text{and} \qquad \eta = \frac{\lambda}{\delta}.$$

The parameter Δ corresponds to the energy of the α transition in figure 12. In the hyperfine expressions, κ is a measure of the core polarization and $P = 2g_N\beta_N\beta\langle r^{-3}\rangle_{3d}$.

Using the principal values of the g matrix (in table 2) and the known $3726\ cm^{-1}$ position of the α band as input, we solved equations (4), (5) and (8) to obtain $k = 0.647$, $\omega = -0.1373$ rad, $\eta = -0.1812$ and $\delta = 2160\ cm^{-1}$. Combining these results with the known $4228\ cm^{-1}$ position of the β band, we then obtained $\mu = 502\ cm^{-1}$ and $10Dq = 2499\ cm^{-1}$. Finally, using the previously determined values for k and ω and taking κ to be 0.20 and $|P|$ to be $102\times10^{-4}\ cm^{-1}$, we solved equations (6) and (7) to obtain estimates of the principal values of the ^{61}Ni hyperfine matrix. These calculations gave $|A_\parallel| = 32.5$ MHz and $|A_\perp| = 84.7$ MHz, which compare reasonably well with our experimental values of $A_\parallel = -60.2$ MHz and $A_\perp = -88.2$ MHz. In general, our values for the various parameters describing Ni^+ in $AgGaSe_2$ are in good agreement with the results of Kaufmann [6] for Ni^+ in the similar compound $AgGaS_2$.

6. Summary

The point defect responsible for the broad, room-temperature absorption band near 2.2 μm in $AgGaSe_2$ is shown to be a Ni^+ ion substituting for a Ag^+ ion. The intensity of this band increases significantly when crystals are doped with Ni. By following the analysis of Kaufmann [6], the positions of zero-phonon lines (4228 and $3726\ cm^{-1}$) observed at low temperature are found to be consistent with the measured g values for Ni^+ if the orbital reduction factor k is near 0.65. We suggest that the performance of optical parametric oscillators utilizing $AgGaSe_2$ and pumped near 2 μm will be improved if Ni^+ impurity ions (even at trace levels) are not present in the crystals.

We also obtained ENDOR data for the central ^{61}Ni nucleus, the four ^{77}Se nearest neighbours, and the four basal plane $^{69,71}Ga$ neighbours. These hyperfine parameters provide information about the nature and extent of the unpaired spin's wavefunction. Estimates of the amount of spin density on the neighbours give 9.5% on the four selenium ions and 2.0% on the four basal-plane gallium ions. Our results, when additional smaller overlaps are taken into account, suggest that approximately 88% of the unpaired spin is localized on the nickel ion. We conclude by noting that all of our data are in agreement with a Ni^+ ion (i.e. a $3d^9$ spin system) having the unpaired spin in the $|xy\rangle$-like orbital, with lobes in the (001) basal plane.

Acknowledgments

This work was supported at West Virginia University and Stanford University by the Air Force Office of Scientific Research (MURI Grant F49620-01-1-0428). Further support at

West Virginia University was provided by the Air Force Office of Scientific Research (Grant F49620-99-1-0248) and the National Science Foundation (Grant DMR-9807128).

References

[1] Bordui P F and Fejer M M 1993 *Annu. Rev. Mater. Sci.* **23** 321
[2] Barnes N P 1995 *Tunable Lasers Handbook* ed F J Duarte (New York: Academic) chapter 7, pp 293–348
[3] Catella G C and Burlage D 1998 *Mater. Res. Soc. Bull.* **23** 28
[4] Catella G C, Shiozawa L R, Hietanen J R, Eckardt R C, Route R K, Feigelson R S, Cooper D G and Marquardt C L 1993 *Appl. Opt.* **32** 3948
[5] Halliburton L E, Giles N C, Schunemann P G and Pollak T M 1996 *J. Appl. Phys.* **79** 556
[6] Kaufmann U 1975 *Phys. Rev.* B **11** 2478
[7] Zheng W C, Wu S Y, Zhao B J and Zhu S F 1999 *Physica* B **269** 319
[8] Kistaiah P, Venudhar Y C, Murthy K S, Iyengar L and Krishna Rao K V 1981 *J. Less-Common Met.* **77** 17
[9] Gonzalez J, Power Ch, Calderon E, Capet F and Munoz A 2001 *Phys. Status Solidi* b **223** 299
[10] Schneider J, Rauber A and Brandt G 1973 *J. Phys. Chem. Solids* **34** 443
[11] Route R K, Feigelson R S, Raymakers R J and Choy M M 1976 *J. Cryst. Growth* **33** 239
[12] Feigelson R S and Route R K 1990 *Mater. Res. Bull.* **25** 1503
[13] Kim N H, Shin D H and Feigelson R S 1996 *Mater. Sci. Eng.* B **38** 229
[14] Morton J R and Preston K F 1978 *J. Magn. Reson.* **30** 577
[15] Weil J A, Bolton J R and Wertz J E 1994 *Electron Paramagnetic Resonance: Elementary Theory and Practical Applications* (New York: Wiley) pp 534–6
[16] Wertz J E and Bolton J R 1972 *Electron Spin Resonance: Elementary Theory and Practical Applications* (New York: McGraw-Hill) pp 320–4